Int. J. Radiation Oncology Biol. Phys., Vol. 77, No. 2, pp. 600–607, 2010

0360-3016/$–see front matter

ELSEVIER

doi:10.1016/j.ijrobp.2009.08.030

PHYSICS CONTRIBUTION

DYNAMIC MULTILEAF COLLIMATOR TRACKING OF RESPIRATORY TARGET MOTION BASED ON A SINGLE KILOVOLTAGE IMAGER DURING ARC RADIOTHERAPY

PER RUGAARD POULSEN, PH.D.,*† BYUNGCHUL CHO, PH.D.,* DAN RUAN, PH.D.,* AMIT SAWANT, PH.D.,* AND PAUL J. KEALL, PH.D.*

*Department of Radiation Oncology, Stanford University, Stanford, California, and †Department of Medical Physics, Department of Oncology, Aarhus University, Aarhus, Denmark

Purpose: To demonstrate and characterize dynamic multileaf collimator (DMLC) tracking of respiratory moving targets that are spatially localized with a single kV X-ray imager during arc radiotherapy.
Methods and Materials: During delivery of an arc field (358° gantry rotation, 72-sec duration, circular field shape), the three-dimensional (3D) position of a fiducial marker in a phantom was estimated in real time from fluoroscopic kV X-ray images acquired orthogonally to the treatment beam axis. A prediction algorithm was applied to account for system latency (570 ms) before the estimated marker position was used for DMLC aperture adaptation. Experiments were performed with 12 patient-measured tumor trajectories that were selected from 160 trajectories (46 patients) and reproduced by a programmable phantom. Offline, the 3D deviation of the estimated phantom position from the actual position was quantified. The two-dimensional (2D) beam-target deviation was quantified as the positional difference between the MLC aperture center and the marker in portal images acquired continuously during experiments. Simulations of imaging and treatment delivery extended the study to all 160 tumor trajectories and to arc treatments of 3-min and 5-min duration.
Results: In the experiments, the mean root-mean-square deviation was 1.8 mm for the 3D target position and 1.5 mm for the 2D aperture position. Simulations agreed with this to within 0.1 mm and resulted in mean 2D root-mean-square beam-target deviations of 1.1 mm for all 160 trajectories for all treatment durations. The deviations were mainly caused by system latency (570 ms).
Conclusions: Single-imager DMLC tracking of respiratory target motion during arc radiotherapy was implemented, providing less than 2-mm geometric uncertainty for most trajectories.

Image-guided radiotherapy, Intrafraction motion, Tumor tracking, Arc radiotherapy.

INTRODUCTION

Intensity-modulated arc therapy (IMAT) allows efficient and highly conformal dose delivery in radiation therapy (1–3). However, IMAT is not readily compatible with gating for management of respiration-induced tumor motion because the treatment interruptions during gated treatments would also require corresponding interruptions and resumptions of the gantry rotation. Tumor tracking, *i.e.*, continuous realignment of the treatment beam to follow the tumor motion, is a more attractive method for intrafraction motion compensation during IMAT, since it maintains high efficiency without treatment interruptions.

To date, tumor tracking has been implemented clinically only for the robotic Cyberknife system (Accuray Inc., Sunnyvale, CA), in which the required intratreatment target position signal is obtained by stereoscopic kV X-ray images of implanted markers (4, 5). For conventional gantry-mounted linear accelerators, dynamic multileaf collimator (DMLC) tracking (6–11) has been demonstrated in phantom experiments with three different input signals for the target position estimation: (1) an external optical system (12), (2) implantable electromagnetic transponders (13, 14), and (3) combined MV portal imaging and orthogonal kV X-ray imaging of an implantable fiducial marker (15).

Reprint requests to: Per Rugaard Poulsen, Stanford University, Department of Radiation Oncology, 875 Blake Wilbur Drive, Stanford, CA 94305-5847. Tel: (650)7243226; Fax: (650) 498 5008; E-mail: ppoulsen@stanford.edu

This work was supported by NCI grant R01CA93626 and by a research grant from Varian Medical Systems, Palo Alto, CA.

Conflict of interest: none.

Acknowledgments—The authors gratefully acknowledge Drs. Sonja Dieterich and Yelin Suh, Stanford University, for the tumor trajectories used in experiments and simulations, Herbert Cattell, Varian Medical Systems, for substantial contributions to the DMLC tracking program, and Hassan Mostafavi and Alexander Sloutsky, Varian Medical Systems, for the marker extraction software used for the off-line analysis of portal images.

Received June 3, 2009, and in revised form Aug 17, 2009. Accepted for publication Aug 17, 2009.

Since the last method relies on marker visibility in the portal images, it is not directly applicable to intensity-modulated treatments, where the marker might be blocked by MLC leaves during part of the treatment. If MV images were not used for the target position estimation, arbitrary beam modulation would be allowed.

Recently, we developed a method for target trajectory estimation from a sequence of X-ray images acquired by a single rotating imager such as the projection images in a cone-beam CT scan (16). For each image in the sequence, the three-dimensional (3D) target position was estimated by combined use of all images in the sequence, both the preceding and the subsequent images. The trajectory estimations with this method were in general very accurate, with root-mean-square (rms) errors typically well below 1 mm for both prostate and lung. Later, a simulation study of prostate trajectories demonstrated that this single-imager method can be extended to real-time application, where only the preceding images are available for target position estimation, with only a modest loss in accuracy (17).

The aim of the present study was to investigate the single-imager method for real-time position estimation of targets undergoing respiratory motion and to integrate it with DMLC tracking of such targets. The geometrical performance of the integrated single-imager DMLC tracking system was investigated in experiments and simulations. The purpose of the simulations was to extend the study to a larger scale than is practically feasible with experiments.

METHODS AND MATERIALS

Experimental DMLC tracking based on a single kV imager

The dataflow during the kV single-imager-based DMLC tracking experiments is shown in Fig. 1. A motion phantom (18) with an embedded fiducial marker was programmed to reproduce a patient-measured tumor trajectory. A 6-MV arc field with 600 monitor units and a 358° counter-clockwise gantry rotation was delivered to the phantom in 72 sec by a Trilogy linear accelerator equipped with a kV on-board imager (OBI) system, a PortalVision AS1000 portal imager system, and a Millennium MLC with 120 leaves (Varian Medical Systems, Palo Alto, CA). The collimator was rotated such that the MLC leaves moved parallel to the craniocaudal (CC) direction. For the purpose of off-line tracking performance analysis, a circular field with a 10-cm diameter was used in the experiments.

During the arc treatment, the 3D target position was estimated online by fluoroscopic kV images acquired at 5 Hz, using the OBI system, which is mounted perpendicular to the treatment beam axis. The kV source-imager-distance was 180 cm, and the exposure settings were 55 kV, 40 mA, and 12 ms. The kV images were stored on the hard disk of the OBI computer, where an in-house-written computer program segmented the fiducial marker by a template-matching algorithm and transmitted the projected target position and the gantry angle at image acquisition to the DMLC tracking program on a dedicated tracking computer (Fig. 1).

In order to enable single-imager DMLC tracking right from treatment onset, a series of pretreatment kV images was acquired in a 23- to 24-sec period just prior to treatment start while the gantry was rotated 120° clockwise and came to a stop at the treatment start angle (179°). Between 115 and 120 pretreatment images were acquired, and DMLC tracking started after image number 100, *i.e.*, typically 3 to 4 sec before treatment onset. The DMLC tracking procedure involved the following four steps for each new kV image:

DMLC tracking procedure, step 1. A 3D Gaussian probability density function (PDF) for the target position was estimated by a maximum likelihood estimation (MLE) method using the current and all previous projections. The pretreatment imaging ensured that enough images were available for this PDF estimation at treatment start. The MLE calculation is an optimization problem in which the Gaussian distribution that maximizes the likelihood of all observed projection images is determined. It was implemented by a conjugate gradient optimization algorithm. The details of the MLE calculation including the objective function are given in the appendix of reference 17.

DMLC tracking procedure, step 2. The 3D target position for the current projection was estimated as the intersection of the 3D Gaussian PDF and the ray line that connects the focus point of the kV source with the projection point on the kV imager (19). When the PDF was estimated for the first time (after 100 images, or 20 sec), this PDF was also used to estimate the 3D target position for all previous images in order to create a training data set for prediction (see below).

DMLC tracking procedure, step 3. A kernel density estimation-based prediction algorithm was applied to estimate the future target position 570 ms after the kV image acquisition. The prediction accounted for the time lag between target motion and the MLC response, which was estimated to be 570 ms, in a separate experiment by a method described previously (15). The prediction algorithm predicted the future target position as a linear combination of the estimated target positions during the preceding 20 sec, thus using a moving temporal window of 20 sec as the training data set.

DMLC tracking procedure, step 4. Finally, the resulting 3D target position estimation was used as input for a real-time DMLC tracking algorithm that dynamically calculated and adjusted the MLC leaf positions as a function of the 3D target position, the delivered dose fraction, gantry angle, and collimator angle (12).

The experiments were performed with 12 representative tumor trajectories that were selected from a database with 160 thoracic and abdominal tumor trajectories (46 patients) estimated by a Cyberknife Synchrony system (Accuray Inc., Sunnyvale, CA) at Georgetown University Hospital, during stereotactic body radiotherapy (20). The tumor trajectories were estimated by the Synchrony system using a correlation model between external patient motion monitored at 25 Hz and implanted fiducial motion monitored by X-ray imaging at intervals of typically 30 to 90 sec. The tumor trajectories for experiments were selected such that they represented the trajectory variations in the motion database such as relatively small motions, large motions in different directions, stable baseline levels, baseline shifts, and a variety of breathing period lengths.

The mean (and range) of the peak-to-peak motion for the 12 trajectories selected for experiments was 4.9 mm (1.2–21 mm) in the left-right (LR) direction, 7.4 mm (0.6–17 mm) in the CC direction, and 4.2 mm (1.4–14 mm) in the anterior-posterior (AP) direction.

Off-line analysis

Several data streams were recorded during each experiment for off-line analysis of the tracking performance. The data and analysis were as follows.

For each kV image, the 3D real-time estimated target position at the moment of imaging was recorded in a log file. This trajectory was compared with the input trajectory for the programmable

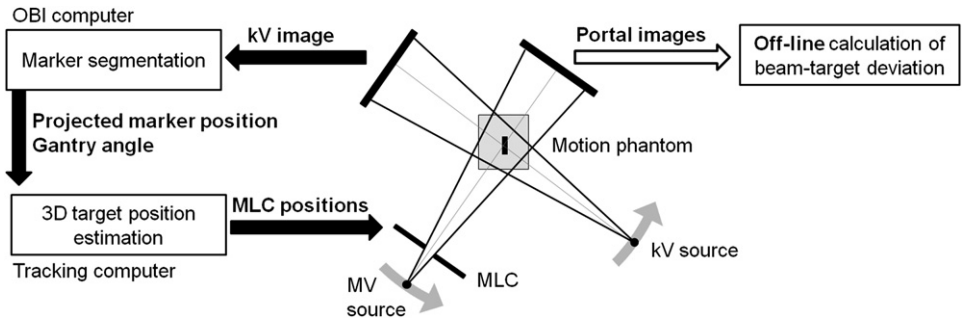

Fig. 1. Data flow and imager configuration for kV single-imager-based DMLC tracking during arc treatment. Black solid arrows indicate real-time data streams for DMLC tracking. The open arrow indicates MV images saved for off-line analysis.

phantom, which was assumed to represent the actual phantom trajectory. The estimated and the actual trajectories were synchronized manually by identifying common features in the CC direction (which was always resolved in the kV images). For each experiment, the position estimation error was determined for all intratreatment kV images and its rms value was calculated. This value is termed the rms deviation of the ''target position estimation at imaging'' throughout this paper.

Also, the predicted 3D target position 570 ms after image acquisition was recorded for each kV image in the log file, and its difference from the phantom input trajectory position at the same time point was calculated. Its rms value is termed the rms deviation of the ''target position estimation at beam correction'' throughout this paper.

Continuous portal images were acquired ~7.5 Hz during the arc treatments. In each image, the marker position was determined by a prototype version of RPM-Fluoro software (Varian Medical Systems), and the center of the circular beam aperture was determined by fitting the aperture to a circle with a 10-cm diameter by a least-squares estimation (13). The difference between the aperture center and the marker position in the portal imager plane was calculated parallel and perpendicular to the MLC leaf direction and scaled to the isocenter distance. For each treatment, the rms of this beam-aperture deviation was calculated by including all portal images.

The planned and actual MLC positions were recorded every 50 ms in Dynalog files (21) during the experiments. The MLC aperture center position was again determined by least-square fitting to a circle with a 10-cm aperture. The planned aperture center position was a series of step functions with time showing abrupt shifts for each new target position estimation. While the Dynalog files specified the planned MLC position steps with a time resolution of 50 ms, only, these position steps were recorded with a time resolution of around 1 ms in the log files generated by the DMLC tracking program. Synchronization of the two log files (recognizing that each recorded step in the Dynalog was a result of a new target position estimation in the DMLC tracking log file in the preceding 0–50 ms time interval) allowed determination of the planned steps in the Dynalog files to within a few milliseconds. Comparison of these planned steps with the actual MLC aperture center position recorded in the Dynalog files was then used to estimate the duration of the MLC adjustments.

Simulations

Simulations were made of each experiment by the DMLC tracking program by performing the same calculations as in the experiments but with simulated rather than measured kV projections as input, and without output connection to the MLC. The simulated kV projections were made with the same projection angles and acquisition times as in the experiments, but a perfect geometry was assumed with no imager flex or marker segmentation uncertainties. As in the experiments, the rms deviation values of the target position estimation at imaging and at beam correction were calculated by comparison with the actual 3D trajectories. Furthermore, the beam-target deviation in the simulations was calculated as the difference between the estimated target position at beam correction and the actual target position after projection onto the MV imager plane.

The results of the 12 simulations were compared with the experimental results in order to investigate the validity of the simulations. Then the simulations of 72-sec arc treatments were made for all 160 thoracic and abdominal tumor trajectories in the database. For all of the 160 trajectories, the mean (and range) of the peak-to-peak motion during the simulated arc treatments was 2.6 mm (0.1–21 mm) in the LR direction, 7.0 mm (0.1–50 mm) in the CC direction, and 3.6 mm (0.2–30 mm) in the AP direction.

Finally, simulations were made for all 160 trajectories for single arc treatments with prolonged durations of 3 and 5 minutes, which would correspond to hypofractionated treatments. The mean peak-to-peak motion was 3.1 mm (LR), 8.3 mm (CC), and 4.3 mm (AP) during the 3-minute treatments and 3.4 mm (LR), 9.0 mm (CC), and 4.7 mm (AP) during the 5-minute treatments. The ranges of peak-to-peak motions were 0.1 to 21 mm (LR), 0.1 to 54 mm (CC), and 0.2 to 32 mm (AP) during both 3- and 5-minute treatments.

RESULTS

Figure 2 shows the phantom trajectories for four selected experiments along with the real-time estimations of the target position at imaging and at beam correction. The target position estimation at imaging (Fig. 2, black curve) agreed fairly well with the phantom trajectory (Fig. 2, green curve). Application of prediction in order to estimate the target position at beam correction (Fig. 2, red curve) clearly introduced some disagreement between estimated and actual target positions (Fig. 2, arrows). After the baseline shifts (Fig. 2d), a few breathing cycles were needed for the prediction algorithm to adapt to a new baseline level.

Figure 3 (two left columns) shows the marker position and the MLC aperture center position in the portal images acquired during the same experiments as in Fig. 2. The difference between the marker and the MLC position is the beam-

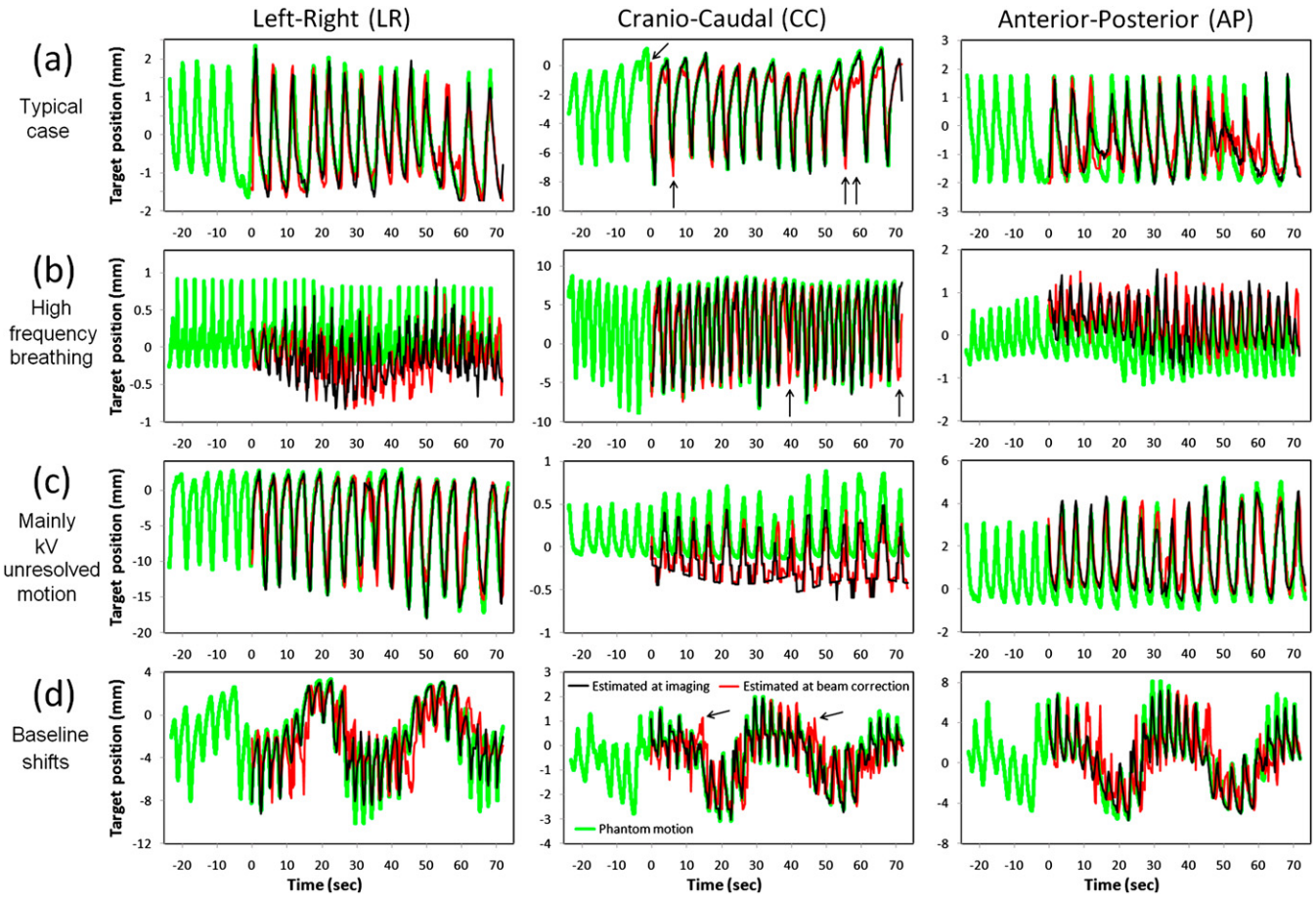

Fig. 2. Experimental results. Four examples of phantom motion in LR, CC, and AP directions during DMLC tracking experiments (green trace). Real-time estimated trajectory at the moment of imaging (black trace) and at the moment of beam correction (*i.e.*, with 570 ms prediction) (red trace). Time $t = 0$, corresponds to treatment onset, $t < 0$ corresponds to pretreatment imaging.

target deviation, whose distribution is shown in the two right columns of Fig. 3. The direction parallel to the MLC corresponds to the CC direction, where the target position was always resolved in the kV images. In this direction, the major discrepancies between the MLC aperture motion and the target motion (Fig. 3, left-column, arrows) can be directly attributed to CC position estimation errors introduced by the prediction (*cf.* Fig. 2, arrows).

In the direction perpendicular to the MLC leaves, the target position was always unresolved in the kV images. Consequently, both the position estimation errors by the single-imager method and the prediction errors contributed to the resulting tracking error. In this direction, the relationship between 3D position estimation errors (Fig. 2) and beam-target deviations (Fig. 3) is less obvious because the beam-target deviation is a result of combined position estimation errors in the LR and AP directions. The examples in Fig. 3b and d represent the experiments with largest rms beam-target deviation parallel and perpendicular to the MLC leaves, respectively.

Table 1 summarizes the mean and maximum rms deviations for all 12 experiments (first two rows) and compares them with the same deviations in the simulations (two lower rows). To facilitate comparison with an optimal nontracking treatment, the last two columns in Table 1 specify the rms intratreatment target position deviation from the mean target position during the pretreatment imaging period. This quantity, which is calculated in a beam's eye view of the treatment beam, represents the uncertainty for an idealized motion-inclusive treatment with perfect setup to the mean tumor position measured just before treatment start. Comparison with the beam-target deviation in the two neighboring columns shows that the tracking reduces the mean rms beam-target deviation by around 60% and 20% in the direction parallel and perpendicular to the MLC, respectively, while the maximum rms beam-target deviation is approximately halved in both directions.

The relationship between experiments and simulations is further detailed in Fig. 4, which shows the individual rms deviations along each direction for each experiment versus the simulated rms deviations. As seen in Fig. 4a, the estimated target position at imaging often had somewhat larger rms deviations in the experiments than in the simulations, which we ascribe to experimental uncertainties in the projected target position determination. On the other hand, good agreement between experiment and simulation values

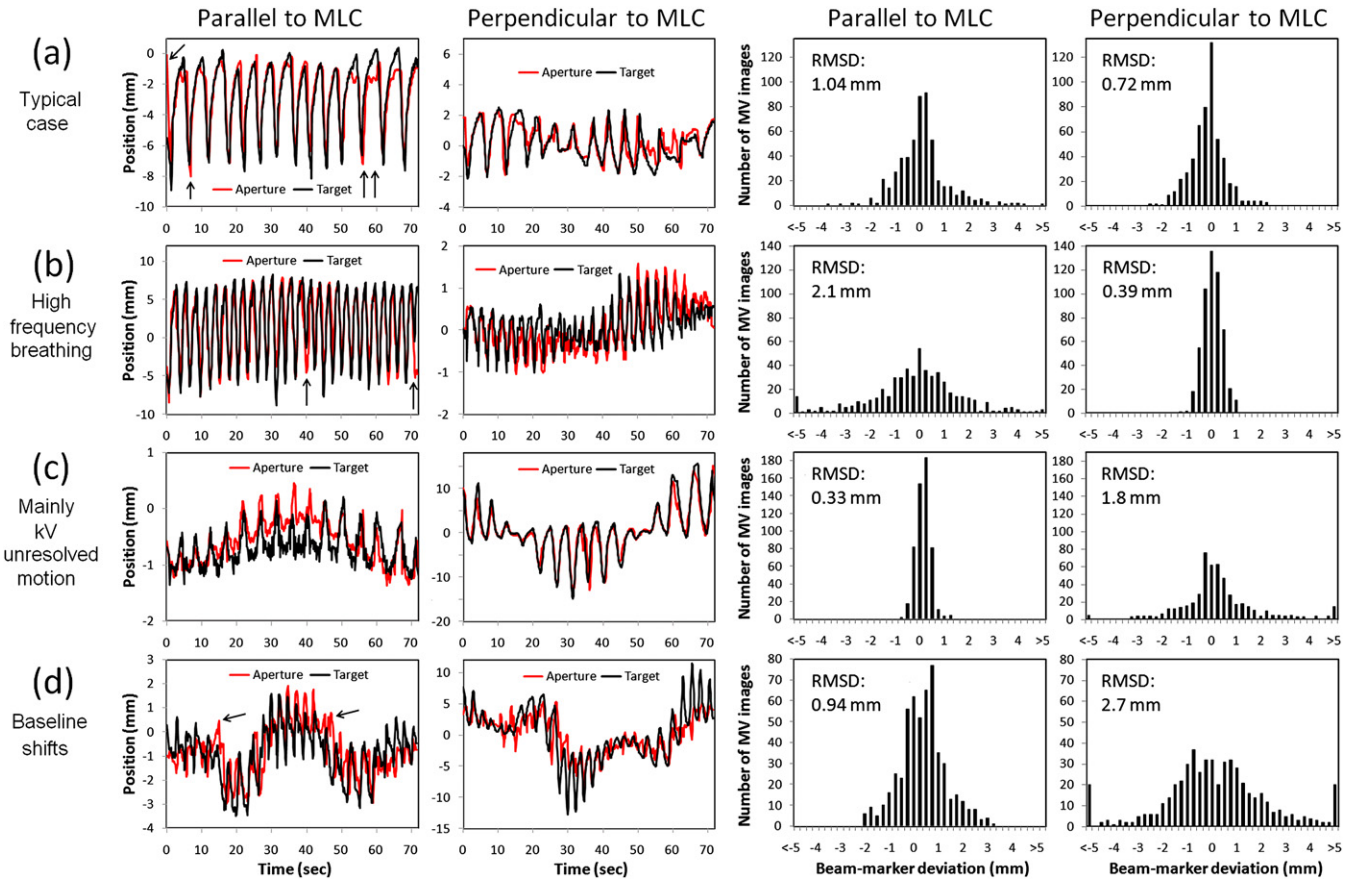

Fig. 3. Experimental results. (Left two columns) Positions of marker (black trace) and beam aperture center (red trace) parallel and perpendicular to the MLC leaves are shown as determined from MV portal images acquired during the four experiments shown in Fig. 2. Note that the vertical scale is different for the two directions. (Right two columns) Distribution of beam-target deviations parallel and perpendicular to the MLC leaves. RMSD = root-mean-square of the beam-target deviation.

was found for the estimated target position at beam correction (Fig. 4b) and for the beam-target deviation (Fig. 4c), because the prediction, which was the main contributor to this deviation, was the same in the simulations as in the experiments.

The good agreement between experimental and simulated deviations shown in Fig. 4 shows that the simulations give good estimates of the experimental deviations except for small deviations below 0.5 mm. It justifies the extension of the simulation to all 160 tumor trajectories. Fig. 5 shows the distribution of rms beam-target deviations in the simulations of 72-sec arc treatments extended to include all 160 trajectories. The mean and maximum rms deviations for these simulations and those for 3- and 5-minute arc treatments are summarized in Table 2, along with the rms tumor position deviation from the pretreatment mean position. Tracking reduces the mean rms beam-target deviation by typically 40% and the maximum rms beam-target deviation by more than 50% compared to the ideal motion inclusive treatment.

Time consumption in experiments

Time stamps in log files created during the experiments showed that the mean time consumption by the marker segmentation program was 38 ms for image file opening and 4 ms for marker segmentation. The mean duration of all procedures by the DMLC tracking program (MLE optimization, 3D target position estimation, prediction, MLC position calculation) varied from 25 ms to 33 ms for the 12 experiments. The total mean time consumption per image by the marker extraction and DMLC tracking programs therefore was 70 to 80 ms.

Analysis of planned and actual MLC aperture positions in the Dynalog files showed that most aperture adaptations to new target positions were completed after around 50 ms, although a few large position adaptations required up to 200 to 250 ms for completion.

This means that around 400 ms of the 570 ms overall system latency from target motion to MLC adaptation originated from the processes leading to an available image file on the hard disk of the OBI computer. Since this includes an average waiting time of 100 ms from target motion to acquisition of the next-coming kV image (due to 5 Hz imaging), we estimate that around 300 ms was spent by the OBI system for image readout, image processing, and image file writing to the hard disk.

Table 1. Mean and maximum rms deviations in the 12 experiments and simulations*

	Position at imaging (mm)				Position at beam correction (mm)				Beam-target deviation (mm)			Target motion (mm)	
Treatment	3D	LR	CC	AP	3D	LR	CC	AP	2D	Parallel	Perp	Parallel	Perp
12 exp, mean	0.69	0.37	0.28	0.49	1.77	0.82	1.06	0.83	1.46	0.86	1.00	1.8	1.2
12 exp, max	1.03	0.80	0.43	0.69	3.7	2.6	2.3	2.5	2.8	2.1	2.7	4.4	4.6
12 sim, mean	0.41	0.29	0.001	0.27	1.70	0.81	0.98	0.76	1.40	0.75	0.98	1.8	1.2
12 sim, max	0.94	0.76	0.003	0.55	3.7	2.5	2.2	2.6	2.6	2.2	2.4	4.4	4.6

Abbreviations: LR = left-right; AP = anterior-posterior; CC = craniocaudal; rms = root-mean-square; 2D = two-dimensional; 3D = three-dimensional; Perp = perpendicular to MLC; exp = experiments; sim = simulations; max = maximum rms deviation.

* Data show mean and maximum rms deviations in the 12 experiments and in simulations. Data include estimated target position deviation at imaging and at beam correction and beam-target deviation parallel and perpendicular to the MLC. Rms target motion in treatment beam's eye view.

DISCUSSION

This study demonstrates that single-imager based DMLC tracking of tumors undergoing respiratory motion can be performed with standard equipment on a modern linear accelerator and that rms beam-target deviations below 2 mm can be obtained for most trajectories.

The accuracy of the current system is limited by the long latency of 570 ms, rather than the restriction to a single X-ray imager. This is obvious from the large difference in position estimation errors at imaging and at beam correction (*i.e.*, before and after prediction [Fig. 4a and b and Tables 1 and 2]). The conditions for the prediction, *i.e.*, relatively sparse target position sampling and a long look-ahead time, are known to be particularly challenging (22). As seen by comparing Fig. 4a and b, latency reductions could be a clear pathway to substantial accuracy improvements.

The time analysis suggests that the main potential for latency reduction would be a faster route from image acquisition to marker segmentation, since this caused more than half of the overall latency. It should be noted that the kV imaging system was not intended for real-time use; an obvious design improvement would be replacement of the image file writing to and reading from the hard disk by direct transfer of the image (or a smaller part of the image) to the OBI computer memory for marker segmentation. Potentially, the overall latency could be halved by such improvements.

The simulated prolonged arc durations of 3 and 5 minutes would allow for hypofractionation with up to ~20 Gy per field for IMAT fields delivered with 1,000 MU/min and a modulation factor of 2. The prolonged treatment duration increased the uncertainty in the 3D position estimation at imaging (Table 2), which is to be expected if the correlation of target motion along different axes changes with time (16). The resulting beam-target deviation, however, did not increase (Table 2), since it was still dominated by the latency. For 3- and 5-minute treatments, the number of intratreatment images is 900 and 1,500, respectively, which could result in a considerable imaging dose to the patient. For comparison, a typical cone-beam CT scan gives around 600 images. The imaging dose might be reduced by reduction of the field size to a small area known to include the target or by use of portal images for target localization when the marker is not blocked by the MLC.

In the experiments, we used a circular MLC aperture because it allows straightforward quantification of the beam-target deviation as the positional difference between

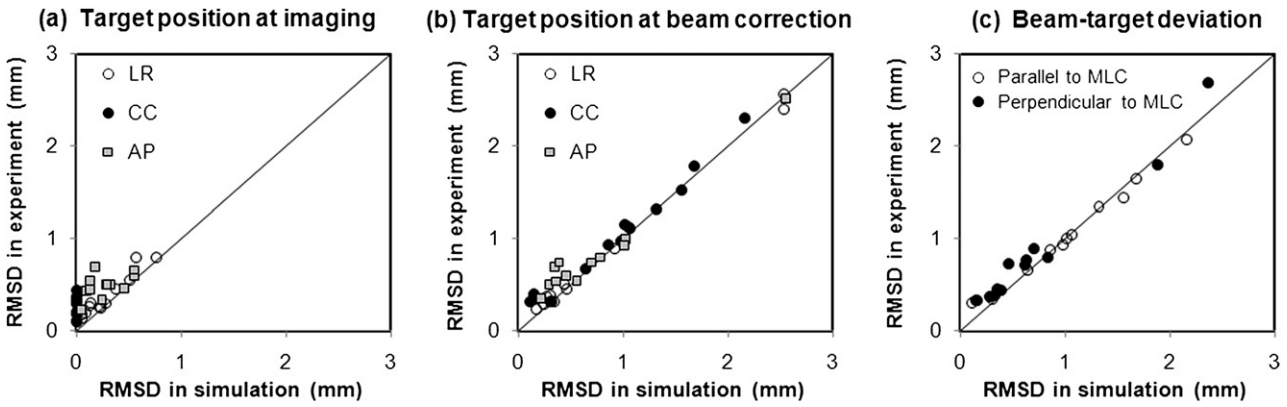

Fig. 4. Comparison of experiments and simulations. Scatter plots showing the root-mean-square deviation (RMSD) in 12 experiments versus the RMSD in simulations of the same experiments. (a) The rms deviation between estimated and actual target position at imaging, (b) rms deviation between estimated and actual target position at beam correction, and (c) rms beam-target deviation in beam's eye view of the treatment beam are shown.

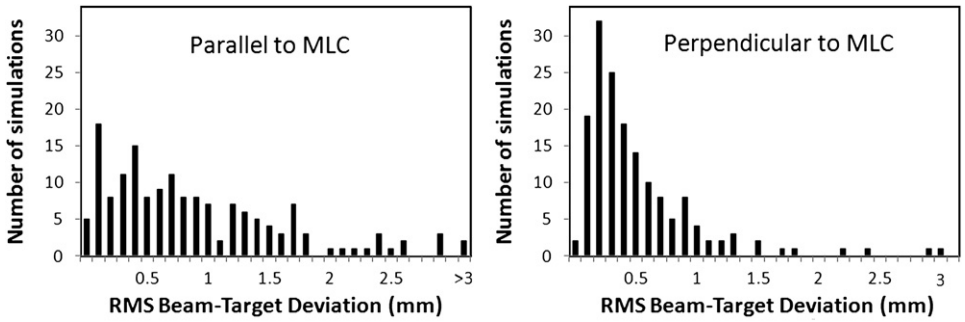

Fig. 5. Simulation results. Distribution of 3D rms beam-target deviations parallel (left panel) and perpendicular (right panel) to the MLC leaves in simulations of 160 arc treatments with 72-sec duration.

the MLC aperture center and the target, since the MLC aperture maintained its circular shape with only little deformation throughout the experiments. For clinical field shapes, which are smaller and more complex, one could expect additional shifts and field aperture deformations caused by the finite leaf width and leaf velocity. We consider this issue, which is common to all DMLC tracking implementations regardless of the target position estimation method, to be beyond the scope of this study.

A major challenge for clinical implementation of the DMLC tracking method is to develop a robust real-time marker segmentation algorithm for clinical kV images. Although robust real-time marker segmentation has been implemented clinically for lung treatments with the Cyberknife system (5), it would be more challenging in a rotational geometry, where the background and relative positions of the projected markers change with the gantry angle. When more than one marker is used, potential problems in identification of each individual marker in the images can be reduced by avoiding marker implantation in the same axial plane.

Limitations of the method for single-imager target position estimation include its dependency on various imaging angles for PDF estimation, *i.e.*, the method is not readily generalized to static gantry angle treatments. This could be overcome by combination with MV images for 3D position estimation (15) or by kV-imaging during pre- and interfield gantry rotations for PDF establishment.

A limitation of this study is that the trajectories used to represent tumor motion were estimated by the Cyberknife Synchrony system by a combination of occasional internal position measurements with continuous external patient motion monitoring, rather than being directly measured continuously (20).This could have exaggerated the motion correlation between tumor motion along different axes, which will improve the performance of the single-imager target position estimation. However, since the overall tracking accuracy was governed by prediction errors, this is not likely to significantly affect the main conclusions and the magnitude of the reported tracking errors.

CONCLUSIONS

In conclusion, DMLC target tracking based on a single imager has been implemented for arc radiotherapy of tumors undergoing respiratory motion. The accuracy of the current implementation is mainly limited by a long system latency of 570 ms. The DMLC tracking method relies on standard equipment for modern linear accelerators. Since MV images are not used for the image-based tracking, the method would allow arbitrary beam modulation.

Table 2. Mean and maximum rms deviations in simulations of 160 arc treatments*

	Position at imaging (mm)				Position at beam correction (mm)				Beam-target deviation (mm)			Target motion (mm)	
Treatment	3D	LR	CC	AP	3D	LR	CC	AP	2D	Parallel	Perp	Parallel	Perp
72 sec, mean	0.26	0.17	0.001	0.18	1.28	0.42	0.92	0.59	1.12	0.92	0.51	1.7	0.9
72 sec, max	1.7	1.3	0.01	1.1	7.9	2.7	6.7	4.0	7.3	6.7	3.0	15	6.2
3 min, mean	0.28	0.18	0.001	0.20	1.29	0.42	0.93	0.58	1.13	0.92	0.51	1.7	0.8
3 min, max	1.2	0.9	0.01	0.8	7.2	2.5	6.1	3.7	6.6	6.1	2.5	13	5.4
5 min, mean	0.32	0.21	0.001	0.22	1.28	0.43	0.93	0.58	1.11	0.93	0.50	1.7	0.8
5 min, max	1.4	1.3	0.02	0.8	6.8	2.3	5.7	3.6	6.2	5.7	2.5	13	5.5

Abbreviations: LR = left-right; AP = anterior-posterior; CC = cranio-caudal; rms = root-mean-square; 2D = two-dimensional; 3D = three-dimensional Perp = perpendicular to MLC; exp = experiments; sim = simulations; max = maximum rms deviation.

* Data show mean and maximum rms deviations in simulations of 160 arc treatments. Data include estimated target position deviation at imaging and at beam correction and beam-target deviation parallel and perpendicular to the MLC. The rms target motion in treatment beam's eye view is shown.

REFERENCES

1. Yu CX. Intensity-modulated arc therapy with dynamic multileaf collimation: An alternative to tomotherapy. *Phys Med Biol* 1995;40:1435–1449.
2. Otto K. Volumetric modulated arc therapy: IMRT in a single gantry arc. *Med Phys* 2008;35:310–317.
3. Wang C, Luan S, Tang G, *et al*. Arc-modulated radiation therapy (AMRT): A single-arc form of intensity-modulated arc therapy. *Phys Med Biol* 2008;53:6291–6303.
4. Schweikard A, Shiomi H, Adler J. Respiration tracking in radiosurgery. *Med Phys* 2004;31:2738–2741.
5. Murphy MJ. Tracking moving organs in real time. *Semin Radiat Oncol* 2004;14:91–100.
6. Keall PJ, Kini VR, Vedam SS, *et al*. Motion adaptive X-ray therapy: A feasibility study. *Phys Med Biol* 2001;46:1–10.
7. Neicu T, Shirato H, Seppenwoolde Y, *et al*. Synchronized moving aperture radiation therapy (SMART): Average tumour trajectory for lung patients. *Phys Med Biol* 2003;48:587–598.
8. Suh Y, Yi B, Ahn S, *et al*. Aperture maneuver with compelled breath (AMC) for moving tumors: A feasibility study with a moving phantom. *Med Phys* 2004;31:760–766.
9. Tacke M, Nill S, Oelfke U. Real-time tracking of tumor motions and deformations along the leaf travel direction with the aid of a synchronized dynamic MLC leaf sequencer. *Phys Med Biol* 2007;52:N505–N512.
10. Papiez L. DMLC leaf-pair optimal control of IMRT delivery for a moving rigid target. *Med Phys* 2004;31:2742–2754.
11. McQuaid D, Webb S. IMRT delivery to a moving target by dynamic MLC tracking: Delivery for targets moving in two dimensions in the beam's eye view. *Phys Med Biol* 2006;51: 4819–4839.
12. Sawant A, Venkat R, Srivastava V, *et al*. Management of three-dimensional intrafraction motion through real-time DMLC tracking. *Med Phys* 2008;35:2050–2061.
13. Sawant A, Smith RL, Venkat RB, *et al*. Toward submillimeter accuracy in the management of intrafraction motion: The integration of real-time internal position monitoring and multileaf collimator target tracking. *Int J Radiat Oncol Biol Phys* 2009;74:575–582.
14. Smith RL, Sawant A, Santanam L, *et al*. Integration of real-time internal electromagnetic position monitoring coupled with dynamic multileaf collimator tracking: An intensity-modulated radiation therapy feasibility study. *Int J Radiat Oncol Biol Phys* 2009;74:868–875.
15. Cho B, Poulsen PR, Sloutsky A, *et al*. First demonstration of combined kV/MV image-guided real-time DMLC target tracking. *Int J Radiat Oncol Biol Phys* 2009;74:859–867.
16. Poulsen PR, Cho B, Keall PJ. A method to estimate mean position, motion magnitude, motion correlation, and trajectory of a tumor from cone-beam CT projections for image-guided radiotherapy. *Int J Radiat Oncol Biol Phys* 2008;72: 1587–1596.
17. Poulsen PR, Cho B, Keall P. Real-time prostate trajectory estimation with a single imager in arc radiotherapy: A simulation study. *Phys Med Biol* 2009;54:4019–4035.
18. Malinowski K, Noel C, Lu W, *et al*. Development of a 4D Phantom for patient-specific, end-to-end radiation therapy QA. *Proc SPIE Int Soc Opt Eng* 2007;6510: 65100E-1–65100E-9.
19. Poulsen PR, Cho B, Langen K, *et al*. Three-dimensional prostate position estimation with a single x-ray imager utilizing the spatial probability density. *Phys Med Biol* 2008;53: 4331–4353.
20. Suh Y, Dieterich S, Cho B, *et al*. An analysis of thoracic and abdominal tumour motion for stereotactic body radiotherapy patients. *Phys Med Biol* 2008;53:3623–3640.
21. Litzenberg DW, Moran JM, Fraass BA. Verification of dynamic and segmental IMRT delivery by dynamic log file analysis. *J Appl Clin Med Phys* 2002;3:63–72.
22. Sharp GC, Jiang SB, Shimizu S, *et al*. Prediction of respiratory tumour motion for real-time image-guided radiotherapy. *Phys Med Biol* 2004;49:425–440.